

# Triplet Probabilistic Embedding for Face Verification and Clustering

Swami Sankaranarayanan

Azadeh Alavi

Carlos Castillo

Rama Chellappa

Center for Automation Research, UMIACS, University of Maryland, College Park, MD 20742

{swamiviv, azadeh, carlos, rama}@umiacs.umd.edu

## Abstract

*Despite significant progress made over the past twenty five years, unconstrained face verification remains a challenging problem. This paper proposes an approach that couples a deep CNN-based approach with a low-dimensional discriminative embedding learned using triplet probability constraints to solve the unconstrained face verification problem. Aside from yielding performance improvements, this embedding provides significant advantages in terms of memory and for post-processing operations like subject specific clustering. Experiments on the challenging IJB-A dataset show that the proposed algorithm performs comparably or better than the state of the art methods in verification and identification metrics, while requiring much less training data and training time. The superior performance of the proposed method on the CFP dataset shows that the representation learned by our deep CNN is robust to extreme pose variation. Furthermore, we demonstrate the robustness of the deep features to challenges including age, pose, blur and clutter by performing simple clustering experiments on both IJB-A and LFW datasets.*

## 1. Introduction

Recently, with the advent of curated face datasets like Labeled faces in the Wild (LFW) [1] and advances in learning algorithms like Deep neural nets, there is more hope that the unconstrained face verification problem can be solved. A face verification algorithm compares two given templates that are typically not seen during training. Research in face verification has progressed well over the past few years, resulting in the saturation of performance on the LFW dataset, yet the problem of unconstrained face verification remains a challenge. This is evident by the performance of traditional algorithms in the publicly available IJB-A dataset ([2], [3]) that was released recently. Moreover, despite the superb performance of CNN-based approaches compared to traditional methods, a drawback of such methods is the long training time needed. In this work, we present a Deep CNN (DCNN) architecture that ensures faster training, and inves-

tigate how much the performance can be improved if we are provided domain specific data. Specifically, our contributions are as follows:

- We propose a deep network architecture and a training scheme that ensures faster training time.
- We formulate a triplet probability embedding learning method to improve the performance of deep features for face verification and subject clustering.

During training, we use a publicly available face dataset to train our deep architecture. Each image is pre-processed and aligned to a canonical view before passing it to our deep network whose features are used as the representation of the image. In the case of IJB-A dataset, the data is divided into 10 splits, each split containing a training set and test set. Hence, to further improve performance, we learn the proposed triplet probability embedding using the training set provided with each split over the features extracted from our DCNN model. During the deployment phase, given a face template, we extract the deep features using the raw CNN model after some automatic pre-processing steps such as face detection and fiducial extraction. The deep features are projected onto a low-dimensional space using the embedding matrix learned during training (note that the projection involves only matrix multiplication). We use the 128-dimensional feature as the final representation of the given face template.

This paper is organized as follows: Section 2 places our work among the recently proposed approaches for face verification. Section 3 details the network architecture and the training scheme. The triplet probabilistic embedding learning method is described in Section 4 followed by results on the IJB-A and CFP datasets and a brief discussion in Section 5. In Section 6, we demonstrate the ability of the proposed method to cluster a media collection from the LFW and IJB-A datasets.

## 2. Related Work

This work broadly consists of two components: the deep network used as a feature extractor and the learning procedure that projects the input features onto a discriminative low-dimensional space. In the past few years, there have

been numerous works in using deep features for tasks related to face verification. The DeepFace [4] approach uses a carefully crafted 3D alignment procedure to preprocess face images and feeds them to a deep network (with 120M parameters) that is trained with a large training set. A kernel classifier is then trained on the resulting features to make the final verification decision. More recently, Facenet [5] uses the inception architecture and a large private dataset to train a deep network using a triplet distance loss function. The training time for this network is of the order of few weeks. Since the release of the IJBA dataset [2], there have been several works that have published verification results for this dataset. Previous approaches presented in [6] and [7] train deep networks using the CASIA-WebFace dataset [8] and the VGG-Face dataset respectively, requiring substantial training time. This paper proposes a network architecture and a training scheme that needs shorter training time and a small query time.

The idea of learning a compact and discriminative representation has been around for decades. Weinberger *et al.* [9] used a Semi Definite Programming (SDP)-based formulation to learn a metric satisfying pairwise and triplet distance constraints in a large margin framework. More recently, this idea has been successfully applied to face verification by integrating the loss function within the deep network architecture ([5], [7]). Joint Bayesian metric learning has been another popular metric used for face verification ([10], [11]). These methods either require a large dataset for convergence or learn a metric directly therefore not amenable to subsequent operations like discriminative clustering or hashing. Classic methods like t-SNE [12], t-STE [13] and Crowd Kernel Learning (CKL) [14] perform extremely well when used to visualize or cluster a given data collection. They either operate on the data matrix directly or the distance matrix generated from the data by generating a large set of pairwise or triplet constraints. The objective of the optimization algorithm is to minimize the violations in the constraint set. While these methods perform very well on a given set of data points, they do not generalize to out-of-sample data. In the current work, we aim to generalize such formulations, to a more traditional classification setting, where domain specific training and testing data is provided. We formulate an optimization problem based on triplet probabilities that performs dimensionality reduction aside from improving the discriminative ability of the test data. The embedding scheme described in this work is a more general framework that can be applied to any setting where labeled training data is available.

### 3. Network Architecture

This section details the architecture and training algorithm for the deep network used in our work. Our architecture consists of 7 convolutional layers with varying kernel sizes.

The initial layers have a larger size rapidly subsampling the image and reducing the parameters while the later layers consist of small filter sizes, which has proved to be very useful in face recognition tasks ([7], [8]). Furthermore, we use the Parametric Rectifier Linear units (PReLU) instead of ReLU, since they allow a negative value for the output based on a learned threshold and have been shown to improve the convergence rate [15].

Layer	Kernel Size/Stride	#params
conv1	11x11/4	35K
pool1	3x3/2	
conv2	5x5/2	614K
pool2	3x3/2	
conv3	3x3/2	885K
conv4	3x3/2	1.3M
conv5	3x3/1	2.3M
conv6	3x3/1	2.3M
conv7	3x3/1	2.3M
pool7	6x6/2	
fc6	1024	18.8M
fc7	512	524K
fc8	10548	10.8M
Softmax Loss		Total: 39.8M

Table 1: Deep Network architecture details

The top three convolutional layers (conv1-conv3) are initialized with the weights from the AlexNet model [16] trained on the ImageNet challenge dataset. Several recent works ([17], [18]) have empirically shown that this transfer of knowledge across different networks, albeit for a different objective, improves performance and more significantly reduces the need to train over a large number of iterations. The compared methods either learn their deep models from scratch ([7], [19]) or finetune only the last layer of fully pre-trained models. The former approach results in large training time and the latter does not generalize well to the task at hand (face verification) and hence resulting in sub optimal performance. In the current work, even though we use a pre-trained model (AlexNet) to initialize the proposed deep network, we do so only for the first three convolutional layers, since they retain more generic information ([17]). Subsequent layers learn representations which are more specific to the task at hand. Thus, to learn more domain specific information, we add 4 convolutional layers each consisting of 512 kernels of size  $3 \times 3$ . The layers conv4-conv7 do not downsample the input thereby learning more complex higher dimensional representations. This hybrid architecture proves to be extremely effective as our raw CNN representation outperforms some very deep CNN models on the IJB-A dataset (Table 2 in Results). In addition, we achieve that performance by training our deep network on the relatively smaller CASIA-WebFace dataset.

The architecture of our network is shown in Figure 1. Layers conv4-conv7 and the fully connected layers *fc6-fc8* are initialized from scratch using random Gaussian distributions. PReLU activation functions are added between each layer. Since the network is used as a feature extractor, the

last layer  $fc8$  is removed during deployment, thus reducing the number of parameters to 29M. The inputs to the network are  $227 \times 227 \times 3$  RGB images. When the network is deployed, the features are extracted from the  $fc7$  layers resulting in a dimensionality of 512. The network is trained using the Softmax loss function for multiclass classification using the Caffe deep learning platform [20].

#### 4. Learning a Discriminative Embedding

In this section, we describe our algorithm for learning a low-dimensional embedding such that the resulting projections are more discriminative. Aside from an improved performance, this embedding provides significant advantages in terms of memory and enables post-processing operations like visualization and clustering.

Consider a triplet  $t := (v_i, v_j, v_k)$ , where  $v_i$  (anchor) and  $v_j$  (positive) are from the same class, but  $v_k$  (negative) belongs to a different class. Consider a function  $S_W : \mathbb{R}^N \times \mathbb{R}^N \mapsto \mathbb{R}$  that is parameterized by the matrix  $\mathbf{W} \in \mathbb{R}^{n \times N}$ , that measures the similarity between two vectors  $v_i, v_j \in \mathbb{R}^N$ . Ideally, for all triplets  $t$  that exist in the training set, we would like the following constraint to be satisfied:

$$S_W(v_i, v_j) > S_W(v_i, v_k) \quad (1)$$

Thus, the probability of a given triplet  $t$  satisfying (1) can be written as:

$$p_{ijk} = \frac{e^{S_W(v_i, v_j)}}{e^{S_W(v_i, v_j)} + e^{S_W(v_i, v_k)}} \quad (2)$$

The specific form of the similarity function is given as:  $S_W(v_i, v_j) = (\mathbf{W}v_i)^T \cdot (\mathbf{W}v_j)$ . In our case,  $v_i$  and  $v_j$  are deep features normalized to unit length. To learn the embedding  $\mathbf{W}$  from a given set of triplets  $\mathbb{T}$ , we solve the following optimization:

$$\underset{\mathbf{W}}{\operatorname{argmin}} \sum_{(v_i, v_j, v_k) \in \mathbb{T}} -\log(p_{ijk}) \quad (3)$$

(3) can be interpreted as maximizing the likelihood (1) or minimizing the negative log-likelihood (NLL) over the triplet set  $\mathbb{T}$ . In practice, the above problem is solved in a Large-Margin framework using Stochastic Gradient Descent (SGD) and the triplets are sampled online. The gradient update for the  $\mathbf{W}$  is given as:

$$\begin{aligned} \mathbf{W}_{\tau+1} = \mathbf{W}_\tau - \eta * \mathbf{W}_\tau * (1 - p_{ijk}) * (v_i(v_j - v_k)^T \\ + (v_j - v_k)v_i^T) \end{aligned} \quad (4)$$

where  $\mathbf{W}_\tau$  is the estimate at iteration  $\tau$ ,  $\mathbf{W}_{\tau+1}$  is the updated estimate,  $(v_i, v_j, v_k)$  is the triplet sampled at the current iteration and  $\eta$  is the learning rate.

By choosing the dimension of  $\mathbf{W}$  as  $n \times N$  with  $n < N$ , we achieve dimensionality reduction in addition to better

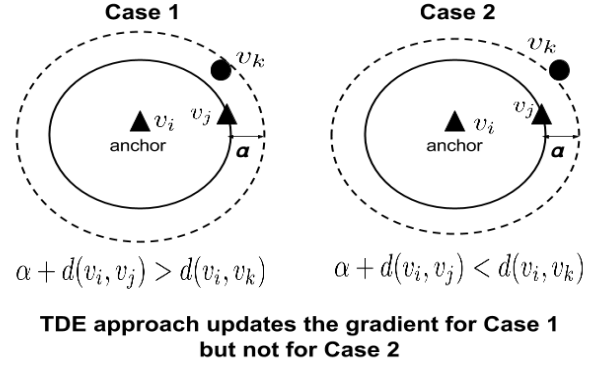


Figure 1: Gradient update scenarios for the TDE method (5). The notation is explained in the text

performance. For our work, we fix  $n = 128$  based on cross validation and  $N = 512$  is the dimensionality of our deep features.  $\mathbf{W}$  is initialized with the first  $n$  principal components of the training data. At each iteration, a random anchor and a random positive data point are chosen. To choose the negative, we perform hard negative mining, ie. we choose the data point that has the least likelihood (2) among the randomly chosen 2000 negative instances at each iteration.

Since we compute the embedding matrix  $\mathbf{W}$  by optimizing over triplet probabilities, we call this method Triplet Probability Embedding (TPE). The technique closest to the one presented in this section, which is used in recent works ([5],[7]) computes the embedding  $\mathbf{W}$  based on satisfying a hinge loss constraint:

$$\underset{\mathbf{W}}{\operatorname{argmin}} \sum_{(v_i, v_j, v_k) \in \mathbb{T}} \max\{0, \alpha + (v_i - v_j)^T \mathbf{W}^T \mathbf{W} (v_i - v_j) - (v_i - v_k)^T \mathbf{W}^T \mathbf{W} (v_i - v_k)\} \quad (5)$$

$\alpha$  acts a margin parameter for the loss function. To be consistent with the terminology used in this paper, we call it Triplet Distance Embedding (TDE). To appreciate the difference between the two approaches, let us look at the gradient update step for (5):

$$\begin{aligned} \mathbf{W}_{\tau+1} = \mathbf{W}_\tau - \eta * \mathbf{W}_\tau * ((v_i - v_j)(v_i - v_j)^T \\ - (v_i - v_k)(v_i - v_k)^T) \end{aligned} \quad (6)$$

Figure 1 shows the case where the gradient update for the TDE method (6) occurs. If the value of  $\alpha$  is not appropriately chosen, a triplet is considered good even if the positive and negative are very close to one another. But under the proposed formulation, both cases referred to in Figure 1 will update the gradient but their contribution to the gradient will be modulated by the probability with which they violate the constraint in (1). This modulation factor is specified by the  $(1 - p_{ijk})$  term in the gradient update for TPE in

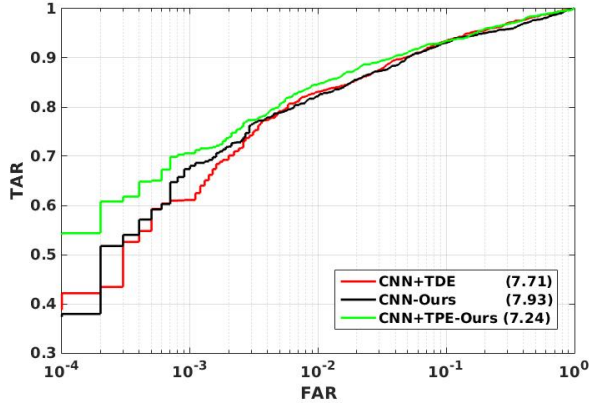


Figure 2: Performance improvement on IJB-A split 1: FAR (vs) TAR plot. EER values are specified in brackets.

(4) implying that if the likelihood of a sampled triplet satisfying (1) is high, then the gradient update is given a lower weight and vice-versa. Thus, in our method, the margin parameter ( $\alpha$ ) is automatically set based on the likelihood. To compare the relative performances of the raw features before projection, with TDE and with TPE (proposed method), we plot the traditional ROC curve (TAR (vs) FAR) for split 1 of the IJB-A verify protocol for the three methods in Figure 2. The Equal Error Rate (EER) metric, which is a popular measure to compare classification systems is specified for each method. The performance improvement due to TPE is significant, especially at regions of  $\text{FAR} = \{10^{-4}, 10^{-3}\}$ . We observed a similar behaviour for all the ten splits of the IJB-A dataset.

## 5. Experimental setup and Results

In this section we evaluate the proposed method on two challenging datasets:

1. **IARPA Janus Benchmark-A (IJB-A) [2]:** This dataset contains 500 subjects with a total of 25,813 images (5,399 still images and 20,414 video frames sampled with a rate of 1 in 60). The faces in the IJB-A dataset contain extreme poses and illuminations, much harder than LFW [1]. An additional challenge of the IJB-A verification protocol is that the template comparisons include image to image, image to set and set to set comparisons. In this work, if a given test template of the IJB-A data we perform two kinds of pooling to produce its final representation:

- Average pooling ( $\text{CNN}_{ave}$ ): The deep features of the images and/or frames present in the template are combined by taking a componentwise average to produce one feature vector. Thus each feature equally contributes to the final representation.
- Media pooling ( $\text{CNN}_{media}$ ): The deep features are combined keeping in mind the media source they come from. The metadata provided with IJB-A gives

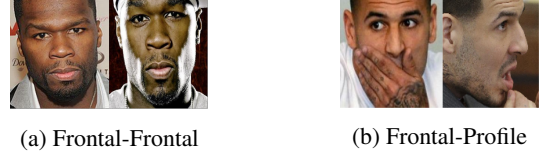


Figure 3: Sample comparison pairs from the CFP dataset



Figure 4: Images from the IJB-A dataset

us the *media id* for each item of the template. Thus to get the final feature vector, we first take an intra-media average and then combine these by taking the inter-media average. Thus each feature's contribution to the final representation is weighted based on its source.

Some sample images from the IJB-A dataset are shown in Figure 4.

2. **Celebrities in Frontal-Profile (CFP) [21]:** This dataset contains 7000 images of 500 people. The dataset is used for evaluating how face verification approaches handle pose variation. Hence, it consists of 5000 images in frontal view and 2000 images in extreme profile. The data is organized into 10 splits, each containing equal number of frontal-frontal and frontal-profile comparisons. Sample comparison pairs of the CFP dataset are shown in Figure 3.

### 5.1. Pre-processing

In the training phase, given an input image, we use the HyperFace method [22] for face detection and fiducial point extraction. The HyperFace detector automatically extracts all the faces from a given image. For the IJB-A dataset, since most images contain more than one face, we use the bounding boxes provided along with the dataset to select the person of interest from the list of automatic detections. We select the detection that has the maximum area overlap with the manually provided bounding box. In the IJB-A dataset, there are few images for which the HyperFace detector cannot find the relevant face. For the missed cases, we crop the face using the bounding box information provided with the dataset and pass it to HyperFace to extract fiducials. We use six fiducial points (eyes and mouth corners) to align the detected image to a canonical view using the similarity transform. For the CFP dataset, since the six keypoints cannot be computed for profile faces we only use three keypoints on one side of the face for aligning them.

### 5.2. Parameters and training times

The training of the proposed deep architecture is done using SGD with momentum, which is set to 0.9 and the learning rate is set to  $1e-3$  and decreased uniformly by a factor of 10

Method	IJB-A Verification (FNMR@FMR)			IJB-A Identification			
	0.001	0.01	0.1	FPIR=0.01	FPIR=0.1	Rank=1	Rank=10
GOTS [2]	0.8 (0.008)	0.59 (0.014)	0.37 (0.023)	0.047 (0.02)	0.235 (0.03)	0.443 (0.02)	-
VGG-Face [7]	0.396 (0.06)	0.195 (0.03)	0.063(0.01)	0.46 (0.07)	0.67 (0.03)	0.913 (0.01)	<b>0.981 (0.005)</b>
Masi <i>et al.</i> [23]	0.275	0.118	-	-	-	0.902	0.968
NAN [19]	0.215 (0.03)	0.103 (0.01)	0.041 (0.005)	-	-	-	-
CNN <sub>ave</sub> (Ours)	0.287 (0.05)	0.146 (0.01)	0.051 (0.006)	0.626 (0.06)	0.795 (0.02)	0.90 (0.01)	0.974 (0.004)
CNN <sub>media</sub> (Ours)	0.234 (0.02)	0.129 (0.01)	0.048 (0.005)	0.67 (0.05)	0.82 (0.013)	0.925 (0.01)	0.978 (0.005)
CNN <sub>media</sub> +TPE (Ours)	<b>0.187 (0.02)</b>	<b>0.10 (0.01)</b>	<b>0.036 (0.005)</b>	<b>0.753 (0.03)</b>	<b>0.863 (0.014)</b>	<b>0.932 (0.01)</b>	0.977 (0.005)

Table 2: Identification and Verification results on the IJB-A dataset. For identification, the scores reported are TPIR values at the indicated points. The results are averages over 10 splits and the standard deviation is given in the brackets for methods which have reported them. ‘-’ implies that the result is not reported for that method. The best results are given in bold.

Algorithm	Frontal-Frontal			Frontal-Profile		
	Accuracy	EER	AUC	Accuracy	EER	AUC
Sengupta <i>et al.</i> [21]	96.40 (0.69)	3.48 (0.67)	99.43 (0.31)	84.91 (1.82)	14.97 (1.98)	93.00 (1.55)
Human Accuracy	96.24 (0.67)	5.34 (1.79)	98.19 (1.13)	<b>94.57 (1.10)</b>	<b>5.02 (1.07)</b>	<b>98.92 (0.46)</b>
CNN (Ours)	<b>96.93 (0.61)</b>	<b>2.51 (0.81)</b>	<b>99.68 (0.16)</b>	89.17 (2.35)	8.85 (0.99)	97.00 (0.53)

Table 3: Results on the CFP dataset [21]. The numbers are averaged over ten test splits and the numbers in brackets indicate standard deviations of those runs. The best results are given in bold.

every 50K iterations. The weight decay is set to  $5e-4$  for all layers. The training batch size is set to 256. The training time for our deep network is 24 hours on a single NVIDIA TitanX GPU. For the IJB-A dataset, we use the training data provided with each split to obtain the triplet embedding which takes 3 mins per split. This is the only additional splitwise processing that is done by the proposed approach. During deployment, the average enrollment time per image after pre-processing, including alignment and feature extraction is 8ms.

### 5.3. Evaluation Pipeline

Given an image, we pre-process it as described in Section 5.1. The deep features are computed as an average of the image and its flip. Given two face images to compare, we compute their cosine similarity score. More specifically, for the IJB-A dataset, given a template containing multiple faces, we *flatten* the template features by average pooling or media pooling to obtain a vector representation. For each split, we learn the TPE projection using the provided training data. The final representation is obtained as:  $y = \mathbf{W}x$ , where  $x$  is the deep feature and  $\mathbf{W}$  is the TPE projection matrix. Given two templates for comparison, we compute the cosine similarity score using the projected 128-d representations.

### 5.4. Evaluation Metrics

We report two types of results for the IJB-A dataset: Verification and Identification. For the verification protocol, we report the False Non-Match Rate (FNMR) values at several

False Match Rates (FMR). For the identification results, we report open set and closed set metrics. The True Positive Identification Rate quantifies the fraction of subjects that are classified correctly among the ones that exist in probe but not in gallery. For the closed set metrics, we report the CMC numbers at different values of False Positive Identification Rates (FPIRs) and Ranks. More details on the evaluation metrics for the IJB-A protocol can be found in [2].

For the CFP dataset, following the protocol set in [21], we report the Area under the curve (AUC) and Equal Error Rate (EER) values as averages across splits, in addition to the classification accuracy. To obtain the accuracy for each split, we threshold our CNN similarity scores where the threshold is set to the value that provides highest classification accuracy over the training data for each split.

### 5.5. Discussion

#### Performance on IJB-A

Table 2 presents the results for the proposed methods compared to existing results for the IJB-A Verification and Identification protocol. The compared methods are described below:

- Government-of-the-Shelf (GOTS) [2] is the baseline performance provided along with the IJB-A dataset.
- Parkhi *et al.* [7] train a very deep network (22 layers) over the VGG-Face dataset which contains 2.6M images from 2622 subjects.
- The Neural Aggregation network (NAN) [19] is trained over large amount of videos from the CELEB-1000

FMR	Ours	Crosswhite <i>et al.</i> [26]
1e-2	0.10 (0.012)	0.061 (0.013)
1e-1	0.036 (0.005)	0.017 (0.007)

Table 4: Recent results on the IJB-A verification protocol. Reported as FNMR at FMR

dataset [24] starting from the GoogleNet [25] architecture. Furthermore, a separate siamese network is trained for verification experiments starting from the NAN network.

- Masi *et al.* [23] use a deep CNN based approach that includes a combination of in-plane aligned images, 3D rendered images to augment their performance. The 3D rendered images are also generated during test time per template comparison, which results in a large query time per template comparison.

Compared to these methods, the proposed method trains a single CNN model on the CASIA-WebFace dataset which consists of about 500K images and requires much shorter training time and has a very fast query time (0.08s after face detection per image pair). Our raw CNN features after media pooling have the best performance among the compared methods in Table 2 in the IJB-A verification and identification protocols with the exception of Rank-10 accuracy where we are very close to the best result. The TPE method provides significant improvement for both the identification and verification tasks as shown in Table 2.

During the preparation of this manuscript, the authors became aware of a recent result on the IJB-A verification protocol. This is shown in Table 4 in comparison with our approach. The method by Crosswhite *et al.* [26] uses the VGG-Face network [7] descriptors (4096-d) as the raw features. They use the concept of template adaptation [27] to improve their performance as follows: when pooling multiple faces of a given template, they train a linear SVM with the features of this template as positive and a fixed set of negatives extracted from the training data of the IJB-A splits. Let’s denote the pooled template feature and classifier pair as  $(t, w)$ . Then, at query time when comparing two templates  $(t_1, w_1)$  and  $(t_2, w_2)$ , the similarity score is computed as:  $\frac{1}{2}(t_1 \cdot w_2 + t_2 \cdot w_1)$ . Even when using a carefully engineered fast linear classifier training algorithm, this procedure increases the run time of the pooling procedure and hence the query time per template comparison significantly. In contrast, our approach requires a matrix multiplication and a vector dot product per comparison. By using a simple neural network architecture, a relatively smaller training dataset and a fast embedding method we have realized a faster and more efficient end-to-end system. To improve our performance further, we are currently incorporating the use of video data into our approach.

## Performance on CFP

On the CFP dataset, we set a new state-of-art on both Frontal-Frontal and Frontal-Profile comparisons, the latter by a large margin. More specifically, for the Frontal-Profile case, we manage to reduce the error rate by **40.8%**. It should be noted that for a fair comparison we have used our raw CNN features without performing TPE. This shows that the raw CNN features we learn are effective even at extreme pose variations.

## 6. Clustering Faces

This section illustrates how the proposed TPE method can be used to cluster a given data collection. We perform two clustering experiments:

1. We perform clustering on the entire LFW [1] dataset that consists of 13233 images of 5749 subjects. It should be noted that about 4069 subjects have only one image.
2. We use the IJB-A dataset and cluster the templates corresponding to the query set for each split the IJB-A verify protocol.

For evaluating the clustering results, we use the metrics defined in [28]. These are summarized below:

- *Pairwise Precision* ( $P_{pair}$ ): The fraction of pairs of samples within a cluster among all possible pairs which are of the same class, over the total number of same cluster pairs.
- *Pairwise Recall* ( $R_{pair}$ ): The fraction of pairs of samples within a class among all possible pairs which are placed in the same cluster, over the total number of same-class pairs.

Using these metrics, the  $F_1$ -score is computed as:

$$F_1 = \frac{2 * P_{pair} * R_{pair}}{R_{pair} + P_{pair}} \quad (7)$$

The simplest way we found to demonstrate the effectiveness of our deep features and the proposed TPE method, is to use the standard MATLAB implementation of the agglomerative clustering algorithm with the average linkage metric. We use the cosine similarity as our basic clustering metric. The simple clustering algorithm that we have used here has computational complexity of  $O(N^2)$ . In its current form, this does not scale to large datasets with millions of images. We believe this is not an insurmountable limitation and we are currently working on a more efficient and scalable (yet approximate) version of this algorithm.

### 6.1. Clustering LFW

The images in the LFW dataset are pre-processed as described in Section 5.1. For each image and its flip, the deep features are extracted using the proposed architecture and their component-wise average normalized to unit  $L_2$  norm is used as the final representation. We run the clustering

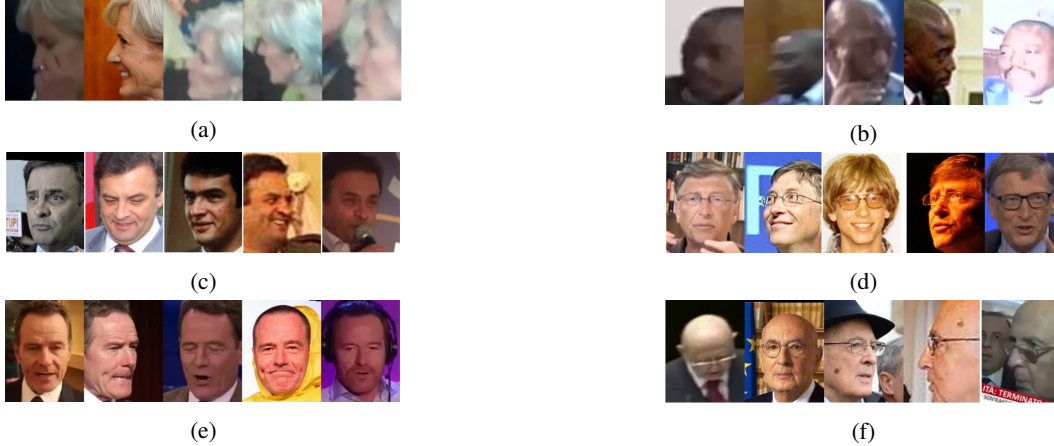


Figure 5: Sample clusters output from the Clustering approach discussed in Section 6 for the data from the split 1 of the IJB-A dataset. Top row (a,b) shows robustness to pose and blur; Middle row (c,d) contains clusters that are robust to age; Bottom row (e,f) shows instances that are robust to disguise.

Method	$F_1$ -score	Clusters
[28]	0.87	6508
CNN (Ours)	<b>0.955</b>	5351

Table 5:  $F_1$ -score for comparison of the two clustering schemes on the LFW dataset. The ground truth cluster number is 5749.

Method	$F_1$ -score	Clusters	After Pruning
CNN <sub>media</sub>	0.79	293 (22)	173
CNN <sub>media</sub> +TPE	<b>0.843</b>	258(17)	167

Table 6: Clustering metrics over the IJB-A 1:1 protocol. The standard deviation is indicated in brackets. The ground truth subjects per each split is 167.

algorithm over the entire data in a single shot. The clustering algorithm takes as input a cut-off parameter which acts as a distance threshold (below which any two clusters will not be merged). In our experiments, we vary this cut-off parameter over a small range and evaluate the resulting clustering using the  $F_1$ -score. We pick the result that yields the best  $F_1$ -score. Table 5 shows the result of our approach and compares it to a recently released clustering approach based on approximate Rank-order clustering [28]. It should be noted that, in the case of [28], the clustering result is chosen by varying the number of clusters and picking the one with the best  $F_1$ -score. In our approach, we vary the cut-off threshold which is the property of the deep features and hence is a more intuitive parameter to tune. We see from Table 5 that aside from better performance, our total cluster estimate is closer to the ground truth value of 5749 than [28].

## 6.2. Clustering IJB-A

The IJB-A dataset is processed as described in Section 5. In this section, we aim to cluster the query templates provided with each split for the verify protocol. We report the results of two experiments: with the raw CNN features (CNN<sub>media</sub> in Table 2) and with the projected CNN features, where the projection matrix is learned through the proposed TPE method (CNN<sub>media</sub>+TPE in Table 2). The cut-off threshold required for our clustering algorithm is learned automatically based on the training data, i.e. we choose the threshold that gives the maximum  $F_1$ -score over the training data. The scores reported in Table 6 are average values over ten splits. As expected, the TPE method improves the clustering performance of our raw features. The subject estimate is the number of clusters produced as a direct result of our clustering algorithm. The pruned estimate is obtained by ignoring the clusters which have less than 3 images.

For a more complete evaluation of our performance over varying threshold values, we plot the Precision-Recall (PR) curve for the IJB-A clustering experiment in Figure 6. As can be observed, the PR curve for clustering the IJB-A data using embedded features exhibits a better performance at all operating points. This is a more transparent evaluation than reporting only the  $F_1$  score since the latter effectively fixes the operating point but the PR curve reveals the performance at all operating points.

## 7. Conclusion and Future Work

In this paper, we proposed a deep CNN-based approach coupled with a low-dimensional discriminative embedding learned using triplet probability constraints in a large margin fashion. The proposed pipeline enables a faster training time and improves face verification performance especially



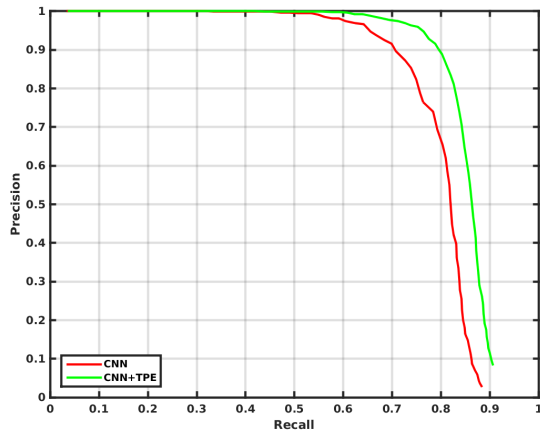


Figure 6: Precision-Recall curve plotted over cut-off threshold varied from 0 to 1.

at low FMRs. We demonstrated the effectiveness of the proposed method on two challenging datasets: IJB-A and CFP and achieved performance competitive with the state of the art while using a deep model which is more compact and trained using a moderately sized dataset. We demonstrated the robustness of our features using a simple clustering algorithm on the LFW and IJB-A datasets. For future work, we plan to use videos directly during training and also embed our TPE approach into training the deep network. We intend to scale our clustering algorithm to handle large scale scenarios such as large impostor sets of the order of millions.

## 8. Acknowledgement

This research is based upon work supported by the Office of the Director of National Intelligence (ODNI), Intelligence Advanced Research Projects Activity (IARPA), via IARPA R&D Contract No. 2014-14071600012. The views and conclusions contained herein are those of the authors and should not be interpreted as necessarily representing the official policies or endorsements, either expressed or implied, of the ODNI, IARPA, or the U.S. Government. The U.S. Government is authorized to reproduce and distribute reprints for Governmental purposes notwithstanding any copyright annotation thereon.

## References

- [1] G. B. Huang, M. Ramesh, T. Berg, and E. Learned-Miller, "Labeled faces in the wild: A database for studying face recognition in unconstrained environments," October 2007.
- [2] B. F. Klare, E. Taborsky, A. Blanton, J. Cheney, K. Allen, P. Grother, A. Mah, M. Burge, and A. K. Jain, "Pushing the frontiers of unconstrained face detection and recognition: Iarpa janus benchmark a," *algorithms*, vol. 13, p. 4, 2015.
- [3] J.-C. Chen, S. Sankaranarayanan, V. M. Patel, and R. Chellappa, "Unconstrained face verification using fisher vectors computed from frontalized faces," *BTAS*, 2015.
- [4] Y. Taigman, M. Yang, M. Ranzato, and L. Wolf, "Deepface: Closing the gap to human-level performance in face verification," in *CVPR 2014*, pp. 1701–1708, IEEE, 2014.
- [5] F. Schroff, D. Kalenichenko, and J. Philbin, "Facenet: A unified embedding for face recognition and clustering," in *CVPR*, 2015.
- [6] D. Wang, C. Otto, and A. K. Jain, "Face search at scale: 80 million gallery," *arXiv preprint arXiv:1507.07242*, 2015.
- [7] O. M. Parkhi, A. Vedaldi, and A. Zisserman, "Deep face recognition," *BMVC*, 2015.
- [8] D. Yi, Z. Lei, S. Liao, and S. Z. Li, "Learning face representation from scratch," *arXiv preprint arXiv:1411.7923*, 2014.
- [9] K. Q. Weinberger, J. Blitzer, and L. K. Saul, "Distance metric learning for large margin nearest neighbor classification," in *NIPS*, 2005.
- [10] K. Simonyan, O. M. Parkhi, A. Vedaldi, and A. Zisserman, "Fisher Vector Faces in the Wild," in *BMVC*, 2013.
- [11] J.-C. Chen, V. M. Patel, and R. Chellappa, "Unconstrained face verification using deep cnn features," *arXiv preprint arXiv:1508.01722*, 2015.
- [12] L. Van der Maaten and G. Hinton, "Visualizing data using t-sne," *JMLR*, vol. 9, no. 2579-2605, p. 85, 2008.
- [13] L. Van Der Maaten and K. Weinberger, "Stochastic triplet embedding," in *Machine Learning for Signal Processing (MLSP), 2012 IEEE International Workshop on*, pp. 1–6, IEEE, 2012.
- [14] O. Tamuz, C. Liu, S. Belongie, O. Shamir, and A. T. Kalai, "Adaptively learning the crowd kernel," *arXiv preprint arXiv:1105.1033*, 2011.
- [15] K. He, X. Zhang, S. Ren, and J. Sun, "Delving deep into rectifiers: Surpassing human-level performance on imagenet classification," *arXiv preprint arXiv:1502.01852*, 2015.
- [16] A. Krizhevsky, I. Sutskever, and G. E. Hinton, "Imagenet classification with deep convolutional neural networks," in *NIPS*, 2012.
- [17] J. Yosinski, J. Clune, Y. Bengio, and H. Lipson, "How transferable are features in deep neural networks?," in *NIPS*, 2014.
- [18] M. Long and J. Wang, "Learning transferable features with deep adaptation networks," *arXiv preprint arXiv:1502.02791*, 2015.
- [19] J. Yang, P. Ren, D. Chen, F. Wen, H. Li, and G. Hua, "Neural aggregation network for video face recognition," *arXiv preprint arXiv:1603.05474*, 2016.



- [20] Y. Jia, E. Shelhamer, J. Donahue, S. Karayev, J. Long, R. Girshick, S. Guadarrama, and T. Darrell, "Caffe: Convolutional architecture for fast feature embedding," *arXiv preprint arXiv:1408.5093*, 2014.
- [21] S. Sengupta, J.-C. Chen, C. D. Castillo, V. M. Patel, R. Chellappa, and D. W. Jacobs, "Frontal to profile face verification in the wild," in *WACV*, 2016.
- [22] R. Ranjan, V. M. Patel, and R. Chellappa, "Hyperfacer: A deep multi-task learning framework for face detection, landmark localization, pose estimation, and gender recognition," *arXiv preprint arXiv:1603.01249*, 2016.
- [23] I. Masi, A. T. Tran, J. T. Leksut, T. Hassner, and G. Medioni, "Do we really need to collect millions of faces for effective face recognition?," *arXiv preprint arXiv:1603.07057*, 2016.
- [24] L. Liu, L. Zhang, H. Liu, and S. Yan, "Toward large-population face identification in unconstrained videos," *IEEE Transactions on Circuits and Systems for Video Technology*, vol. 24, pp. 1874–1884, Nov 2014.
- [25] C. Szegedy, W. Liu, Y. Jia, P. Sermanet, S. Reed, D. Anguelov, D. Erhan, V. Vanhoucke, and A. Rabinovich, "Going deeper with convolutions," in *CVPR*, 2015.
- [26] N. Crosswhite, J. Byrne, O. M. Parkhi, C. Stauffer, Q. Cao, and A. Zisserman, "Template adaptation for face verification and identification," *arXiv preprint arXiv:1603.03958*, 2016.
- [27] L. Wolf, T. Hassner, and Y. Taigman, "The one-shot similarity kernel," in *ICCV*, 2009.
- [28] C. Otto, D. Wang, and A. K. Jain, "Clustering millions of faces by identity," *arXiv preprint arXiv:1604.00989*, 2016.